J Solid State Electrochem (2011) 15:1235–1242
DOI 10.1007/s10008-010-1182-x

ORIGINAL PAPER

Carbon nanotube arrays supported manganese oxide and its application in electrochemical capacitors

Dan-Dan Zhao · Zhi Yang · Eric Siu-Wai Kong · Cai-Ling Xu · Ya-Fei Zhang

Received: 10 May 2010 / Revised: 15 August 2010 / Accepted: 25 August 2010 / Published online: 18 September 2010

Abstract Manganese oxide (MnO_x) has been coated on carbon nanotubes (CNTs) and fabricated as the electrodes for electrochemical capacitors (ECs) by cathodic electrodeposition. In the process, randomly oriented CNT arrays are grown directly onto the Ti/Si substrates by chemical vapor deposition method. Potentiostatic method has been utilized for cathodic electrodeposition of MnO_x onto the surface of CNTs while immersed in $KMnO_4$ solution. The highly porosity and fibrous microstructure of the as-prepared MnO_x/CNT electrode is beneficial for the electrolyte access to the active material, whereas CNTs provide improved electronic conductivity. Electrochemical investigations show that the increase in the loading mass of MnO_x results in a significant reduction in the specific capacitances (SCs) of the MnO_x/CNT electrodes. The MnO_x/CNT electrode with MnO_x loading mass of 50 μg shows a high SC of 400 Fg^{-1} with good long cycle stability at a current density of 10 Ag^{-1}, suggesting its potential application in ECs.

Keywords Electrochemical capacitors · MnO_x/CNT nanocomposites · Chemical vapor deposition · Potentiostatic cathodic electrodeposition · Electrochemical properties

Introduction

In recent years, electrochemical capacitors (ECs), devices capable of storing charges in the electrode/electrolyte interface, have received much attention due to their higher power density and longer cycle life compared to secondary batteries and higher energy density vis-a-vis conventional electrical double-layer capacitors [1]. In particular, ECs based on hydrous ruthenium oxides exhibit much higher specific capacitances (SCs) compared to conventional carbon materials and are much more stable than electronically conducting polymer materials [2]. However, the high cost of this noble metal material limits its further commercial application. Hence, much effort has been aimed at searching for alternative inexpensive electrode materials with good capacitive characteristics, e.g., transition metal oxides, such as MnO_x [3], NiO_x [4, 5], CoO_x [6], etc.

MnO_x has been considered as a promising electrode material for ECs because of its low cost and excellent capacitive performance in the aqueous electrolytes [7]. Due to the low conductivity of MnO_x, the SC values reported in the literature are usually in the range between 100 and 250 Fg^{-1} [8]. Carbon nanotubes (CNTs) can be a perfect conducting additive or support for materials with pseudo-capacitance properties [9–11]. Therefore, many efforts have been made in the area of the fabrication of MnO_x/CNT composite materials, where improved electronic conductiv-

Electronic supplementary material The online version of this article (doi:10.1007/s10008-010-1182-x) contains supplementary material, which is available to authorized users.

D.-D. Zhao · Z. Yang (✉) · E. S.-W. Kong · Y.-F. Zhang (✉)
Key Laboratory for Thin Film and Microfabrication Technology of the Ministry of Education, National Key Laboratory of Micro/Nano Fabrication Technology, Research Institute of Micro/Nanometer Science and Technology,
Shanghai Jiao Tong University,
Shanghai 200240, China
e-mail: zhiyang@sjtu.edu.cn
e-mail: yfzhang@sjtu.edu.cn

D.-D. Zhao · C.-L. Xu
Key Laboratory of Nonferrous Metal Chemistry and Resources Utilization of Gansu Province, College of Chemistry and Chemical Engineering, Lanzhou University,
Lanzhou 730000, China

ity has been achieved by the use of CNT powders [12] or CNT arrays grown directly on the substrates [13, 14]. It is worthwhile to mention that CNT arrays grown directly on the current collectors of ECs by chemical vapor deposition (CVD) method offer the advantage of having low contact resistance, which is important for the fabrication of efficient EC electrode with high capacitive rates. Additionally, this approach is characteristic with binder-free processing: the use of binder is undesirable for the fabrication of composite electrodes, since binder can be attributed to cause an increased resistance and reduced SC [15].

Electrochemical deposition techniques show unique principles and flexibility in the control of the structure and morphology of nanomaterials, such as offering smaller particle size and agglomerate-free processing [16]. Significant interests have been generated in application of electrochemical deposition methods for the fabrication of MnO_x/CNT composite electrodes. There are some reports on anodic electrodeposition of MnO_x on the CNT powders [17, 18] or the CNT arrays [15] from $MnSO_4$ solution. In another study [19], manganese hydroxide has been electrodeposited cathodically from $Mn(CH_3COO)_2$ solution on the CNT arrays and then converts to γ-MnO_2 after annealing at 350 °C. To avoid the anodic oxidation and dissolution of the low-cost metallic current collectors and to offer the advantage of room-temperature processing, MnO_x has been electrodeposited on randomly oriented CNT arrays by cathodic reduction of Mn^{7+} species from $KMnO_4$ solution, using the following reaction [20]:

$$MnO_4^- + 2H_2O + 3e^- \rightarrow MnO_2 \downarrow + 4OH^- \quad (1)$$

The use of the randomly oriented CNT arrays is beneficial for the electrolyte access to the whole CNT surface during electrodeposition of MnO_x [20]. In contrast, due to the limited ion access to the CNT surface and electrical shielding effect of the vertically aligned CNT arrays, the MnO_x particles form only at the junctions of the individual CNTs [15].

In this investigation, randomly oriented CNT arrays are grown directly onto the Ti/Si substrates by CVD method. For the first time, potentiostatic method has been utilized for cathodic electrodeposition of MnO_x onto CNTs in $KMnO_4$ solution. The MnO_x/CNT electrodes are physically characterized by field-emission scanning electron microscopy (FESEM), transmission electron microscopy (TEM), X-ray diffraction (XRD), and energy dispersive spectroscopy (EDS). Electrochemical capacitance performance of the electrodes has been investigated by means of cyclic voltammetry (CV) and galvanostatic charge–discharge tests in 0.5 M Na_2SO_4 aqueous solution electrolyte. A SC of 400 $F g^{-1}$ at specific current density as high as 10 $A g^{-1}$ is obtained for the MnO_x/CNT electrode with MnO_x loading mass of 50 μg, suggesting that the MnO_x/CNT electrode is potentially a good candidate for EC applications.

Experimental

Preparation of the MnO_x/CNT electrode

Firstly, a thin layer (~50 nm) of Ti was deposited by alternate current magnetron sputtering on Si wafer to form a Ti/Si substrate. Then, a thin layer (~50 nm) of Fe was deposited by direct current magnetron sputtering to serve as the catalyst for the growth of CNTs. The randomly oriented CNT arrays were grown directly onto the Ti/Si substrate at 700 °C in a CVD reactor [21]. A pressure of about 400 Pa was maintained by flowing acetylene, hydrogen, and argon gases with a total flow rate of 180 sccm (volume ratio 5:3:10) during 1 h growing process. By measuring the weight difference of the substrates with and without CNTs, the mass of about 0.50 mg was obtained by a Sartorius BS21S semimicro balance (Germany) for the CNTs synthesized on the Ti/Si substrate with a geometric surface area of about 5 cm^2. Consequently, for the CNTs synthesized on the Ti/Si substrate with a geometric surface area of about 0.5 cm^2, the mass of CNTs was estimated to be approximately 50 μg.

The cathodic electrodeposition of MnO_x was performed using the potentiostatic method. The as-grown CNT electrode was used as the cathode, while a platinum electrode was selected as the anode. A saturated calomel electrode (SCE) was used as the reference electrode. The electrolyte used in this investigation was 20 mM $KMnO_4$ aqueous solution in a standard three-electrode glass cell. MnO_x was electrodeposited at a fixed potential of −0.80 V vs. SCE under coulometric control using a Chenhua CHI660 model Electrochemical Workstation (China) at room temperature. To prepare the MnO_x/CNT electrode with a loading mass of 50 μg MnO_x, the corresponding deposition charge quantity was approximately 0.1665 C as estimated by Faraday's law on the hypothesis that the efficiency of MnO_x deposition was 100%. The deposition efficiency was investigated by electrochemical quartz crystal microbalance technique (EQCM). A three-electrode cell included a platinum-coated AT-cut quartz crystal working electrode, a platinum counter electrode and a SCE. The mass of MnO_x deposit was obtained using a Princeton Applied Research QCM 922 quartz crystal microbalance (QCM, USA). The experimental data obtained from EQCM study showed that the deposition efficiency was approximately 100% (Fig. S1). After deposition, the MnO_x/CNT electrodes were rinsed with high purity water and dried at room temperature in air.

Characterization

The microstructure, nanostructure, and morphology of the as-prepared electrodes were investigated by a Carl Zeiss Ultra 55 FESEM (Germany) and a JEM-2100 TEM (Japan). The crystal structure and phase content of the MnO_x/CNT electrode were studied by a Bruker D8 Advance XRD (Germany) with Cu $K\alpha$ radiation (λ= 1.5418 Å) at an angle (2θ) speed of $6°\,min^{-1}$ and an EDS attached to the FESEM. The capacitive properties of the as-prepared electrodes were investigated by CV and chronopotentiometry method on the Chenhua CHI660 model Electrochemical Workstation at room temperature. The electrochemical impedance spectroscopy (EIS) investigations were performed in the frequency range of 10 mHz–100 kHz at a voltage of 5 mV. A typical three-electrode electrochemical cell was employed, containing 0.5 M Na_2SO_4 aqueous solution as the electrolyte. The as-prepared electrode was used as the working electrode. A platinum foil (area 1 cm^2) was utilized as the counter electrode, while an Ag/AgCl electrode was chosen as the reference electrode. The reproducibility of these experiments was investigated in this work. The variability in data between samples prepared under similar conditions was in the range of ±5%. All chemicals were of analytical grade. High purity water was used throughout.

Results and discussions

Microstructure, morphology, crystal structure, and phase content

FESEM and TEM are employed to obtain direct visualization of surface morphology, microstructure, and nanostructure features of the as-prepared electrodes. Figure 1a, b shows typical FESEM images of CNTs grown directly onto the Ti/Si substrates. The FESEM image at low magnification (Fig. 1a) indicates that CNTs totally cover the Ti/Si substrate surface and have a length of about 10 μm. The CNTs are randomly oriented, entangled, and form a highly porous three-dimensional network, providing necessary intertubular spaces for the transfusion of electrolyte and reactant into the whole CNT electrode. As shown in Fig. 1b, the wall of CNTs is smooth with the average external diameter of 50 nm. The nanotube's inner cavity is readily seen even in low magnification TEM image (Fig. 2a). The wall thickness of CNTs is ~15 nm and the external diameter ranges from 50 to 60 nm, which is consistent with the FESEM results. Moreover, it can be seen from the TEM image at higher magnification (Fig. 2b) that the CNTs have about 40 walls. It is known that the multi-walled CNTs are formed by continuous layers surrounding the central canal, which is favorable for a good electrical conductivity of each nanotube. This entangled network of conducting CNTs should be a perfect support for inexpensive transition metal oxides of poor electrical conductivity, such as amorphous manganese oxide ($MnO_x \cdot yH_2O$) [12].

The MnO_x/CNT electrode is prepared by potentiostatic cathodic electrodeposition method at −0.80 V vs SCE in 20 mM $KMnO_4$ aqueous solution. The corresponding FESEM images are shown in Fig. 1c and d. Similar to the literature [20], the enhanced deposition at the CNT junctions can be observed (Fig. 1c). However, FESEM image indicates that MnO_x particles are also well dispersed on the surface of individual CNT (Fig. 1d). The surface morphology of the individual MnO_x/CNT nanocomposite is investigated by TEM, and the corresponding results are shown in Fig. 2. The surface structure of the MnO_x/CNT nanocomposite is composed of MnO_x nanosheets with length and thickness of 10–40 and 2–4 nm, respectively (Fig. 2a). The TEM image at higher magnification (Fig. 2b) shows that the diameter of individual MnO_x/CNT nanocomposite is about 70–100 nm, which is consonant with the FESEM results. FESEM and TEM investigations reveal the highly porosity and fibrous microstructure of the as-prepared MnO_x/CNT electrode. Besides nanopores in MnO_x coating layer (Fig. 1d), there is a great deal of macropores among composite nanotubes (Fig. 1c and d), which collectively compose a hierarchically porous structure. Such microstructure with small particle size and high surface area is beneficial to ion transport and redox reactions which underlie the charge storage mechanism [12, 22, 23].

In addition to morphology analysis, the crystal structure and the composition of the MnO_x/CNT nanocomposite on Ti/Si substrates are analyzed using XRD and EDS. Figure 3a shows the typical XRD pattern of the as-prepared MnO_x/CNT electrode. Except the Ti/Si substrate peaks, the XRD curve has a very small peak at 2θ around 26.61°, which is the characteristic peak of graphite and should arise from CNTs. The main peaks of the MnO_x can be roughly identified and the amorphous nature of the electrodeposits can be confirmed by the XRD spectrum. Two small and broad peaks at 2θ around 11.81° (001) and 23.77° (002) can be indexed to rancieite-type MnO_2 including an amorphous phase (JCPDS file 22-0718). This result is consistent with the report on the rancieite-type MnO_2 films electrodeposited cathodically from aqueous $KMnO_4$ solution [24]. According to the literature [25], the rancieite structure has the near MnO_2 composition with a general formula of $A_xMnO_{2+y}(H_2O)_z$, in which A represents an alkali metal cation or Ca cation. The peak weakening and broadening probably result from the small grain size and poor crystallinity of a compound, indicating

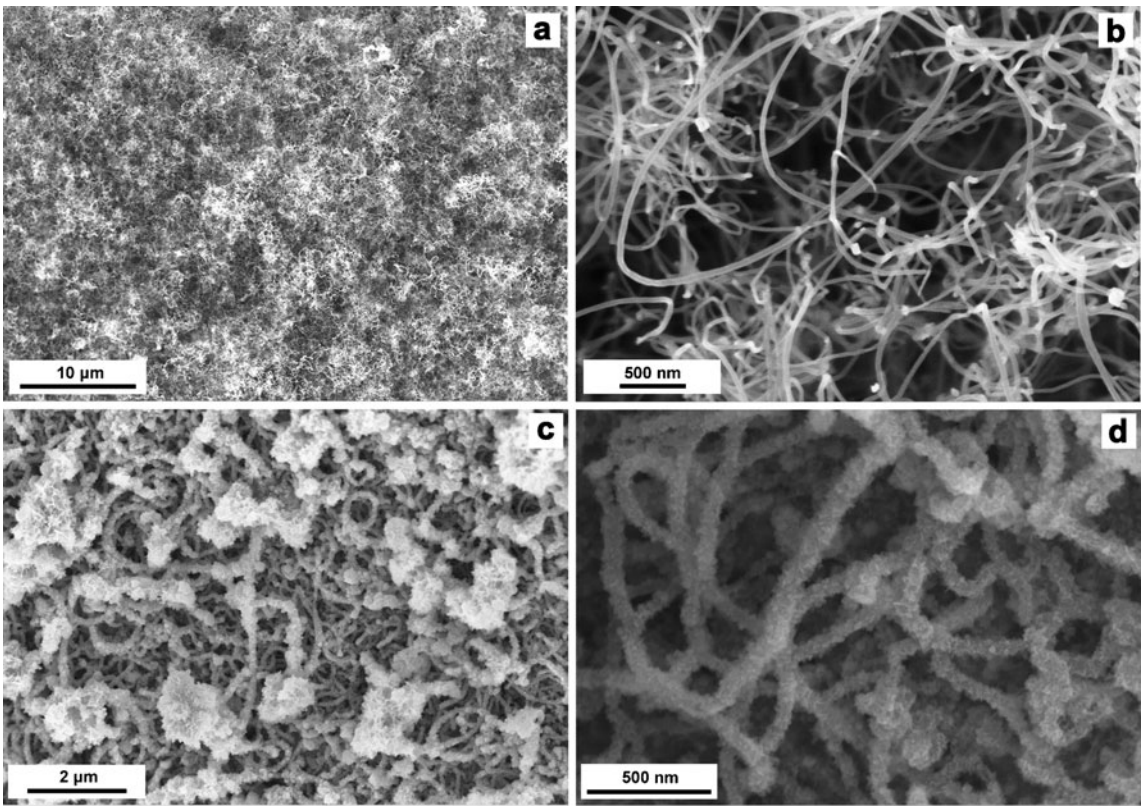

Fig. 1 **a**, **b** FESEM images at different magnifications of the as-grown CNT electrode and **c**, **d** FESEM images at different magnifications of the as-deposited MnO_x/CNT electrode (the loading mass of MnO_x is 50 μg)

the amorphous nature of the electrodeposits. It is known that the amorphous structure will favor the fast proton/ions diffusion rate, which is an important characteristic needed for a metallic oxide to be chosen as an electrode material [12, 22, 23].

Typical EDS data for the as-prepared MnO_x/CNT electrodes are presented in Fig. 3b. EDS analysis of the electrode confirms the presence of Si, Ti (originated from the Ti/Si substrate), C (mainly originated from CNTs), O, Mn, and Na elements (mainly originated from MnO_x). This result is consistent with XRD analysis as mentioned above. Moreover, EDS pattern indicates that the electrodeposits contain Na and Mn species with a Na/Mn atomic ratio of $x=0.33$. This value is in a good agreement with those of the rancieite-type MnO_2 films electrodeposited cathodically from aqueous $KMnO_4$ solutions [24].

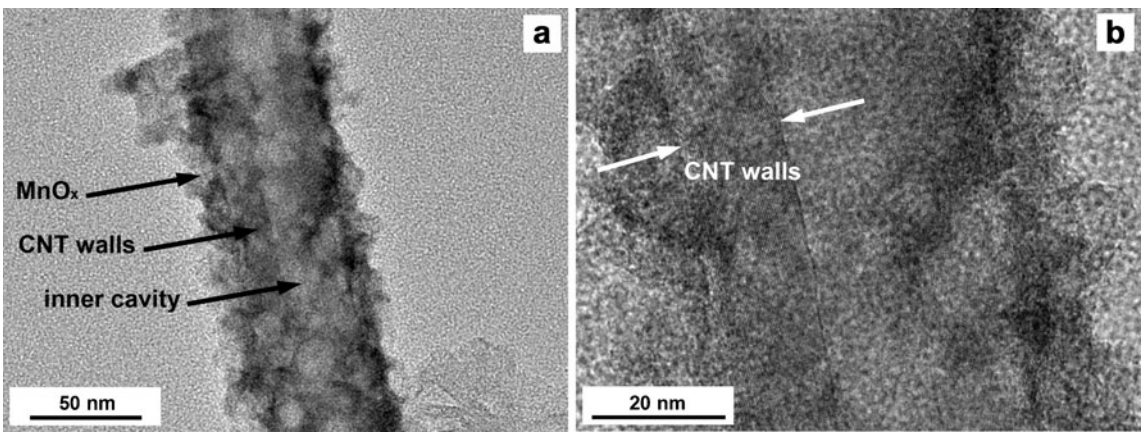

Fig. 2 TEM images of individual MnO_x/CNT nanocomposite with low (**a**) and high (**b**) magnification

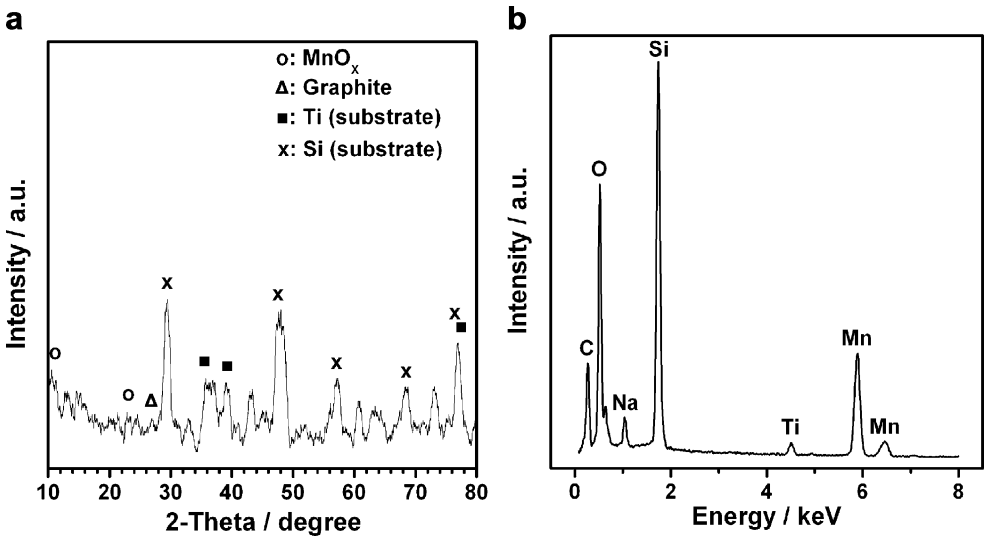

Fig. 3 XRD (**a**) and EDS (**b**) patterns of the as-deposited MnO_x/CNT electrode (*unfilled circles* MnO_x, JCPDS file 22–0718; *unfilled triangles* Graphite, JCPDS file 75–2078; *filled squares* Ti(substrate), JCPDS file 89–5009; and *ex symbols* Si (substrate), JCPDS file 89–5012)

Capacitive properties of the MnO_x/CNT electrodes

According to the literatures [12, 19], the capacitive behavior of MnO_x could be attributed to its surface reversible redox transitions involving protons and/or cations exchange with the electrolyte. The charging mechanism of MnO_x is described by the following equation:

$$\left[MnO_x(OH)_y\right]_{surface} + \delta B^+ + \delta e^- \underset{charge}{\overset{discharge}{\rightleftharpoons}} \left[B_\delta MnO_x(OH)_y\right]_{surface} \quad (2)$$

Where B^+=Li^+, Na^+, K^+, and H^+. $MnO_x(OH)_y$ and $B_\delta MnO_x(OH)_y$ indicates the interfacial MnO_x at the high oxidation state and at the low oxidation states, respectively. Equation 2 indicates that the large surface area and high ionic and electronic conductivity of the electrode material are necessary in order to utilize the high theoretical SC (C_t; 1,110 Fg^{-1}) of MnO_x [19].

CV studies are performed to evaluate the capacitive behaviors of the as-synthesized MnO_x/CNT electrodes. Figure 4 shows the typical CVs (with the specific current densities based on MnO_x) at a scan rate of 10 mVs^{-1} under a potential range from 0 to 1 V for the MnO_x/CNT electrode with MnO_x loading mass of 50 μg (Curve a), the MnO_x film deposited on Ti/Si substrate with MnO_x loading mass of 50 μg (Curve b), and the MnO_x/CNT electrode with MnO_x loading mass of 400 μg (Curve c) in 0.5 M Na_2SO_4 aqueous solution. From Fig. 4, the sweet-potato-shaped CVs can be observed for all the electrodes. The shape of the CV curves reveals that the capacitive characteristic is distinguished from that of pure electric double-layer capacitance in which case it is an ideal rectangular shape. Additionally, the CV shape of the MnO_x/CNT electrode with MnO_x loading mass of 50 μg is obviously larger and broader than that of the MnO_x film electrode with the same loading mass. The results imply that the capacitance properties of MnO_x/CNT nanocomposites are mainly related to MnO_x involved Faradaic process (see Eq. 2), and the MnO_x/CNT electrode has better capacitive performance than the MnO_x film electrode with the same loading mass. Moreover, for the MnO_x/CNT electrode with MnO_x loading mass of 400 μg, its CV shape is much smaller and narrower than those of the electrodes with MnO_x loading mass of 50 μg, suggesting that the increase in the loading mass of MnO_x results in a significant reduction in the SCs.

Figure 5 shows CVs (with the specific current densities based on MnO_x) at different scan rates for the MnO_x/CNT electrode with MnO_x loading mass of 50 μg. Since solution

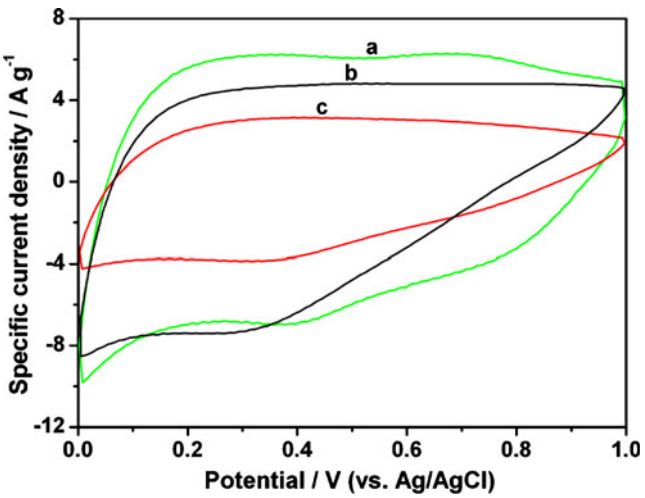

Fig. 4 CVs (with the specific current densities based on MnO_x) at a scan rate of 10 mVs^{-1} in 0.5 M Na_2SO_4 aqueous solution for the MnO_x/CNT electrode with MnO_x loading mass of 50 μg (*Curve a*), the MnO_x film electrode with loading mass of 50 μg (*Curve b*), and the MnO_x/CNT electrode with MnO_x loading mass of 400 μg (*Curve c*)

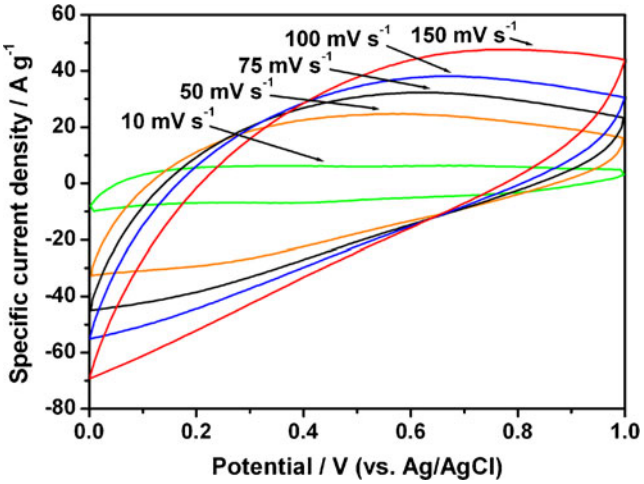

Fig. 5 CVs (with the specific current densities based on MnO_x) at scan rates of 10, 50, 75, 100, and 150 mVs^{-1} for the MnO_x/CNT electrode with MnO_x loading mass of 50 μg

and electrode resistance can distort current response at the switching potential and this distortion is dependent upon the scan rate [22], the shape of the CV has changed with the scan rate increased. These results indicate that the measured capacitance is mainly based on redox mechanism. In order to investigate the electrochemical characteristics of the supercapacitor electrodes/electrolyte interface in a quantitative manner, EIS measurements are performed. The Nyquist plots typically consist of a high frequency semicircle and a low frequency spike (Fig. S2). The high frequency value of the real part of complex impedance has been used for the estimation of the electrode system resistance, which is found to be ~5.72 Ω for the MnO_x/CNT electrode with MnO_x loading mass of 50 μg. The results indicate that the presence of CNTs indeed decreases the resistance of the electrode system. Moreover, the increase in the loading mass of MnO_x results in a significant increase in electrical resistance. The impedance data were analyzed in terms of complex capacitance in order to determine the relaxation time constant (τ_0) (Fig. S3). The relaxation time constant (τ_0) value of ~0.16 s is obtained for the MnO_x/CNT electrode with MnO_x loading mass of 50 μg, suggesting that the charging/discharging process is relatively slow.

The SC of the MnO_x/CNT electrode can be estimated from CVs according to the following equation [19]:

$$C_s = \frac{i}{v \times M} \tag{3}$$

Where i is the CV current density at 0.5 V in the CV anodic branch; v is the CV scan rate; M is the mass of MnO_x (or MnO_x/CNT nanocomposite); C_s is the SC based on MnO_x (or MnO_x/CNT nanocomposite). Figure 6 shows SCs (based on MnO_x) vs. scan rates for the MnO_x/CNT electrode with MnO_x loading mass of 50 μg (Curve a), the MnO_x film electrode with loading mass of 50 μg (Curve b), and the MnO_x/CNT electrode with MnO_x loading mass of 400 μg (Curve c). The MnO_x/CNT electrode with MnO_x loading mass of 50 μg exhibits SC based on MnO_x (or MnO_x/CNT nanocomposite) of 604.4 (or 302.2), 486.0 (or 243.0), 408.3 (or 204.1), 343.6 (or 171.8), and 251.3 (or 125.7) $F\ g^{-1}$ for scan rate of 10, 50, 75, 100, and 150 mVs^{-1}, respectively. Such high SCs indicate that MnO_x has very high dispersibility and usability in MnO_x/CNT electrodes. For the MnO_x film electrode with loading mass of 50 μg, the SC equals to 481.1, 228.5, 160.2, 116.6, and 76.1 Fg^{-1} for scan rate of 10, 50, 75, 100, and 150 mVs^{-1}, respectively. The results indicate that the use of CNT-modified substrates allow higher SCs based on MnO_x, especially at high scan rates, which are similar to those reported in the literature [20]. The improved capacitive behaviors of the MnO_x/CNT electrodes can be attributed to their lower electrical resistance. It is suggested that the porous structure of the MnO_x/CNT electrode (see Fig. 1c and d) is beneficial for the electrolyte access to the active material, whereas CNTs provide improved electronic conductivity. Turning again to Eq. 2, it should be noted that the improved electrolyte access to the active material and good electronic conductivity of the CNT support enable relatively high SCs. Moreover, the MnO_x/CNT electrode with MnO_x loading mass of 400 μg exhibits SC based on MnO_x (or MnO_x/CNT nanocomposite) of 310.3 (or 275.8), 195.6 (or 173.8), 146.1 (or 129.8), 112.8 (or 100.2), and 74.1 (or 65.8) Fg^{-1} for scan rate of 10, 50, 75, 100, and 150 mVs^{-1}, respectively. Obviously, the increase in the loading mass of MnO_x results in a significant reduction in the SCs of the MnO_x/CNT electrode. This also indicates that the stability of the MnO_x/CNT electrode with more

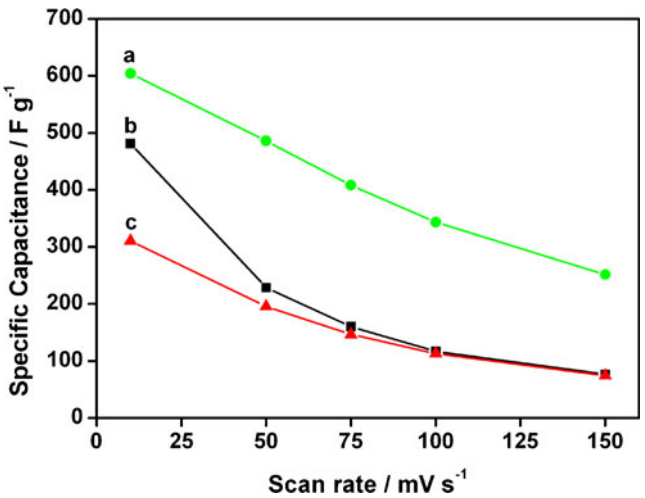

Fig. 6 SCs (based on MnO_x) vs. scan rates for the MnO_x/CNT electrode with MnO_x loading mass of 50 μg (*Curve a*), the MnO_x film electrode with loading mass of 50 μg (*Curve b*), and the MnO_x/CNT electrode with MnO_x loading mass of 400 μg (*Curve c*)

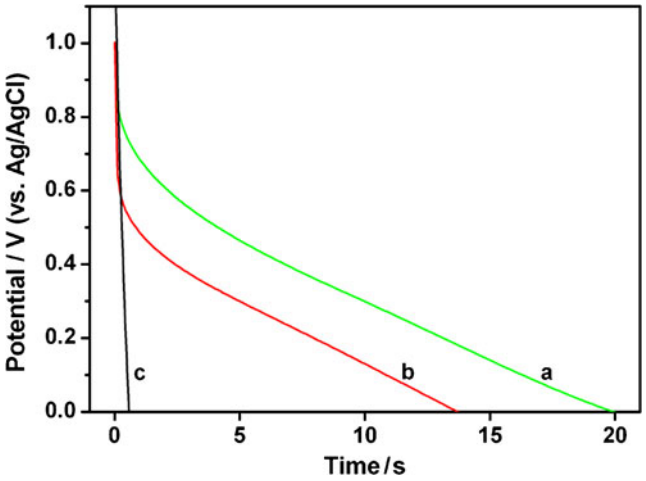

Fig. 7 Discharge curves at a specific current density of 10 Ag^{-1} in 0.5 M Na_2SO_4 aqueous solution for the MnO_x/CNT electrode with MnO_x loading mass of 50 μg (*Curve a*), the MnO_x/CNT electrode with MnO_x loading mass of 400 μg (*Curve b*), and the as-grown CNT electrode (*Curve c*)

loading mass of MnO_x is indeed worse in the entire current regions.

It can be noted that the SCs obtained from voltammograms are deformed by *iR* effect especially at high scan rates. Therefore, the capacitive properties of the MnO_x/CNT electrodes are also investigated by chronopotentiometry and the corresponding results are shown in Fig. 7. It is known that the SC of the electrode for ECs can be efficiently quantified from the galvanostatic discharge curve according to the following equation [22, 23]:

$$C_s = \frac{I \times t}{\Delta V \times M} \tag{4}$$

Where I is the current during discharge process; t is the discharge time; ΔV is the potential window (in this study, ΔV=1 V); M is the mass of MnO_x (or MnO_x/CNT nanocomposite); C_s is the SC of the electrode based on MnO_x (or MnO_x/CNT nanocomposite). The SC calculated from the discharge curves at a specific current density of 10 Ag^{-1} (Fig. 7) for the MnO_x/CNT electrode with MnO_x loading mass of 50 μg is 400.0 (or 200.0) Fg^{-1}, while for the MnO_x/CNT electrode with MnO_x loading mass of 400 μg is 155.0 (or 137.8) Fg^{-1}. Obviously, there has been a significant decrease in the SC as expected when the MnO_x loading mass increases. In addition, the SC of the as-grown CNT electrode equals to 6.0 Fg^{-1} which is too small in comparison with those of the MnO_x/CNT electrodes. The results imply that the MnO_x/CNT electrodes have much better capacitive performance than the CNT electrode, and the SCs of the MnO_x/CNT electrodes arise mainly from MnO_x. The CNTs play the role of mechanical support of MnO_x in the MnO_x/CNT electrodes. It is worthwhile to mention about the *iR* drop which is defined as the electrical potential difference between the two ends of a conducting phase during a current flow and is the product of the current (i) and the resistance (R) of the conductor. As can be seen from Fig. 7, when the MnO_x loading mass increases, the *iR* drop shows a corresponding enlargement, indicating the degradation of the capacitive performance. In other words, the low capacity values related with the increase in the MnO_x loading mass are associated with the *iR* drop within the capacitors. This is mainly because that the increase in the MnO_x loading mass allows the increase in the internal resistance. In the present study, the MnO_x/CNT electrode with MnO_x loading mass of 50 μg shows a smaller *iR* drop, indicating its higher power capability.

The long-term cycle stability of the MnO_x/CNT electrode with MnO_x loading mass of 50 μg is also investigated by the galvanostatic charge–discharge method at a specific current density as high as 10 Ag^{-1} in 0.5 M Na_2SO_4 aqueous solution and the corresponding result is shown in Fig. 8. The inset figure shows typical charge–discharge curves after considerable number of cycles. It can be seen that all curves are near linear and almost symmetrical which implies that the electrode has favorable electrochemical reversibility and charge–discharge properties. The MnO_x/CNT electrode displays good long-term cycle stability, with an efficiency of 88% after 500 charge–discharge cycles, indicating that the repetitive charge–discharges do not induce noticeable degradation of the microstructure. Sometimes, the mechanical properties of electrode materials change due to the ions intercalation/de-intercalation processes. The randomly oriented CNT arrays play the role of mechanical support of the MnO_x nanoparticles in the MnO_x/CNT electrodes. The long entangled CNTs not only inter-connect the MnO_x nanoparticles but also connect the MnO_x nanoparticles with the current collector of the electrode. The

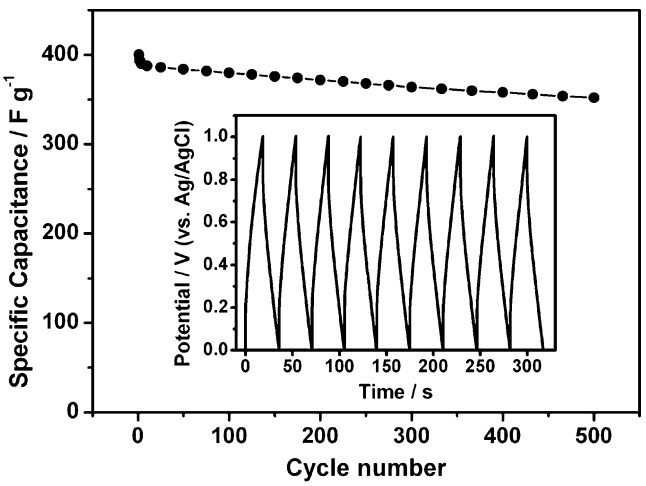

Fig. 8 Long cycle performance of the MnO_x/CNT electrode with MnO_x loading mass of 50 μg at a specific current density of 10 Ag^{-1} in 0.5 M Na_2SO_4 aqueous solution

presence of CNTs in a composite system improves the electronic conductivity and also reduces the stress induced because of cycling [26].

Considering both the SC and the rate capability, the MnO_x/CNT electrode with MnO_x loading mass of 50 μg shows the superior EC performance with a SC value of 400 Fg^{-1} at a specific current density as high as 10 Ag^{-1}. The main reason for the improved electrochemical properties can be attributed to the randomly oriented CNT arrays which connect the MnO_x nanoparticles with the current collector of the electrode to improve the electronic conductivity. The inter connectivity of the MnO_x nanoparticles by CNTs increases the reactivity of MnO_x which are present not only on the surface but also in the interior of the electrode. In addition, the presence of CNTs is expected to greatly reduce the stress induced by the high current cycling, which is very important for a long cycle stability of the system [26].

Conclusions

The results presented in this investigation indicate that CVD method enables the randomly oriented CNT arrays to grow directly onto the Ti/Si substrates and form porous microstructures. Then, MnO_x nanoparticles are successfully electrodeposited on the surface of individual CNT by the potentiostatic cathodic technique which is a simple and room-temperature process, appropriate for the application in low-cost metallic current collectors. The porous microstructure of CNTs formed on the substrates facilitates the access of MnO_4^- ions to the CNT surfaces during electrodeposition. Moreover, the porous microstructure of the MnO_x/CNT nanocomposite is beneficial for the electrolyte access to the active material. In other words, this nanostructure allows us to derive a significant proportion of the capacity from fast bulk redox process, which provides an important basis for the MnO_x/CNT nanocomposite to behave as possible electrode material for ECs. As a result, MnO_x/CNT electrodes with a loading mass of 50 μg of MnO_x show good capacitive behaviors, with a specific capacitance of 400 Fg^{-1} at a specific current density as high as 10 Ag^{-1}. This MnO_x/CNT nanocomposite prepared by CVD and potentiostatic cathodic electrodeposition techniques appears most promisingly to be a potential electrode material for ECs.

Acknowledgements The authors gratefully acknowledge financial support by the National Natural Science Foundation of China (No. 50730008, 50902092, and 20903050), Shanghai Science and Technology Grant (No. 1052nm02000, 09JC1407400, and 1052nm06800), Shanghai Research Fund for the Post-doctoral Program (No. 10R21414700), China Postdoctoral Science Foundation funded project (No. 20100470710), and Interdisciplinary Innovation Research Fund for Young Scholars of Lanzhou University (No. LZUJC2007004).

References

1. Conway BE (1999) Electrochemical supercapacitors—scientific fundamentals and technological applications. Kluwer/Plenum, New York
2. Zheng JP, Cygan PJ, Jow TR (1995) J Electrochem Soc 142:2699
3. Pang SC, Anderson MA, Chapman TW (2000) J Electrochem Soc 147:444
4. Srinivasan V, Weidner JW (1997) J Electrochem Soc 144:L210
5. Zhao D-D, Xu M-W, Zhou W-J, Zhang J, Li H-L (2008) Electrochim Acta 53:2699
6. Lin C, Ritter JA, Popov BN (1998) J Electrochem Soc 145:4097
7. Hu C-C, Tsou TW (2002) Electrochem Commun 4:105
8. Long JW, Young AL, Rolison DR (2003) J Electrochem Soc 150: A1161
9. Iijima S (1991) Nature 354:56
10. Frackowiak E (2007) Phys Chem Chem Phys 9:1774
11. Li Z-J, Wang L, Su Y-J, Liu P, Zhang Y-F (2009) Nano-Micro Lett 1:9
12. Piñero ER, Khomenko V, Frackowiak E, Béguin F (2005) J Electrochem Soc 152:A229
13. Fan Z, Chen J-H, Wang M-Y, Cui K-Z, Zhou H-H, Kuang Y-F (2006) Diam Relat Mater 15:1478
14. Zhang W-D, Chen J (2009) Pure Appl Chem 81:2317
15. Zhang H, Cao G-P, Wang Z-Y, Yang Y-S, Shi Z-J, Gu Z-N (2008) Nano Lett 8:2664
16. Liang C-L, Zhong K, Liu M, Jiang L, Liu S-K, Xing D-D, Li H-Y, Na Y, Zhao W-X, Tong Y-X, Liu P (2010) Nano-Micro Lett 2:6
17. Lee CY, Tsai HM, Chuang HJ, Li SY, Lin P, Tsenga TY (2005) J Electrochem Soc 152:A716
18. Nam KW, Lee CW, Yang XQ, Cho BW, Yoon WS, Kim KB (2009) J Power Sources 188:323
19. Fan Z, Chen J-H, Zhang B, Liu B, Zhong X-X, Kuang Y-F (2008) Diam Relat Mater 17:1943
20. Wang Y-H, Liu H, Sun X-L, Zhitomirskya I (2009) Scr Mater 61:1079
21. Wei S, Kang W-P, Davidson JL, Huang J-H (2008) Diam Relat Mater 17:906
22. Zhao D-D, Bao S-J, Zhou W-J, Li H-L (2007) Electrochem Commun 9:869
23. Zhao D-D, Zhou W-J, Li H-L (2007) Chem Mater 19:3882
24. Wei J, Nagarajan N, Zhitomirsky I (2007) J Mater Process Technol 186:356
25. Leroux F, Guyomard D, Piffard Y (1995) Solid State Ionics 80:299
26. Subramanian V, Zhu H-W, Wei B-Q (2006) Electrochem Commun 8:827